MOLECULAR PHYSICS, 1980, VOL. 39, NO. 1, 239–249

Force and density study of the chemical reaction process $OH_2+H^+\rightarrow OH_3^+$

by T. KOGA†, H. NAKATSUJI, and T. YONEZAWA
Department of Hydrocarbon Chemistry, Faculty of Engineering,
Kyoto University, Kyoto, Japan

(*Received* 19 *October* 1977 ; *in revised form* 2 *January* 1979)

The force and density origin of the ionic reaction process $OH_2+H^+\rightarrow OH_3^+$ is studied on the basis of the electrostatic force theory. In order to obtain reliable results, we have used the floating AO wavefunction (with minimal basis) which satisfies the Hellmann–Feynman theorem for the approaching proton. Accuracies of the results of the ordinary nuclear-centred AO wavefunction (with minimal basis plus polarization functions on hydrogen atoms) have been also examined. It is shown that the predominant origin of the driving force is the atomic dipole force which is caused by the transfer of the lone-pair density of OH_2 into the atomic region of H^+ and the succeeding inward polarization of the transferred electron density. The exchange force due to density accumulation in the forming $O–H^+$ bond region is of secondary importance. This is in contrast with the previous results for the radical reaction processes. The present reaction may be regarded as the transformation of the lone pair into the bond pair.

1. INTRODUCTION

Recently, there has been growing interests in the force approach in theoretical chemistry [1–9]. Based on the electrostatic Hellmann–Feynman theorem [1], the force theory has been successfully applied extensively to fields such as molecular structures, chemical reactions, and long-range forces [1–9], where the simplicity and the visuality of the force concept have been fully utilized.

In a previous paper [3], we have studied the force and density origin of the radical reaction process $NH_2+H\rightarrow NH_3$ on the basis of the electrostatic force (ESF) theory [4, 5]. It was shown that the driving force of the reaction acting on the attacking H nucleus arises primarily from the density accumulated in the N–H overlap region (i.e., the exchange (EC) force between H and N atoms). The force due to the polarization of the atomic density of H, i.e., the atomic dipole (AD) force, was of secondary importance. This feature was common to the radical reactions $H+H\rightarrow H_2$ [6 a] and $CH_3+CH_3\rightarrow C_2H_6$ [4 b] studied earlier.

Here, we study the force and density origin of the reaction, $OH_2+H^+\rightarrow OH_3^+$ in comparison with the previous isoelectronic reaction, $NH_2+H\rightarrow NH_3$. Since the present reaction is essentially ionic and the reactant H^+ produces an electric field at OH_2, a different origin of the driving force of the reaction is

† Present address : Department of Industrial Chemistry, Muroran Institute of Technology, Muroran, Japan.

0026-8976/80/3901 0239 $02·00

expected. Two different wavefunctions have been employed in order to obtain reliable results for the Hellmann–Feynman force acting on the approaching proton. One is the ordinary nuclear-centred AO wavefunction with minimal basis plus polarization functions on the hydrogen atoms and the other the floating 1s(H^+) AO wavefunction with minimal basis set. For the radical reaction $NH_2 + H \rightarrow NH_3$, the wavefunctions of the former type were used ; they have given the forces on the attacking hydrogen with about 70 per cent accuracy [3]. On the other hand, the latter wavefunction has been shown to exactly satisfy the Hellmann–Feynman theorem [5, 7]. The floating wavefunction excludes numerical errors from the Hellmann–Feynman force calculations, and permits a quantitative discussion with simple and visual physical pictures intrinsic to the Hellmann–Feynman theorem [5]. The following section provides the computational methods with some numerical results. Analysis and discussion of the reaction process $OH_2 + H^+ \rightarrow OH_3^+$ are given in § 3 in terms of the partitioned forces (AD, EC, and extended gross charge (EGC) forces) [4 a, e] and the dynamic behaviour of the electron cloud (electron-cloud preceding and electron-cloud incomplete following) [4 c, e].

2. Computational methods and results

We consider that the OH_2 fragment is fixed in space. Then the force acting on the attacking H^+ is our main interest. The geometries of the reactant OH_2 and the product OH_3^+ are taken from the experimental values ; O–H = 0·96 Å and $\angle$ HOH = 105° for OH_2 [10], and 1·02 Å and 117° for OH_3^+ [11].

In the first step, we determine the minimum-energy reaction path (figure 1) and calculate the driving force of the reaction, using the ordinary Hartree–Fock SCF MO method with minimal STO-3G basis [12 a] plus 1G p-type polarization functions on the hydrogen atoms (nuclear-centred AO basis). The

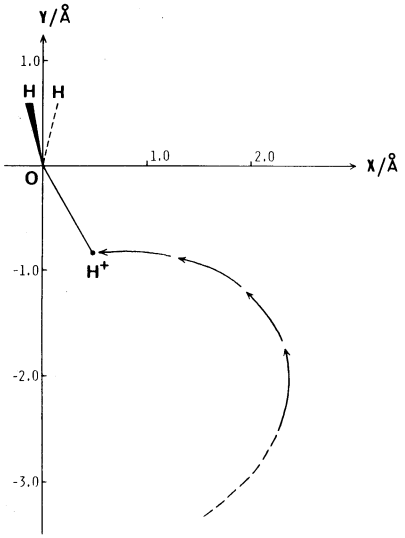

Figure 1. The calculated minimum-energy reaction path for the reaction $OH_2 + H^+ \rightarrow OH_3^+$.

structure of the OH_2 fragment of the system was fixed at that of water. The exponents for the STO-3G basis were taken from the paper of Hehre, Stewart, and Pople [12 b]. The exponent of the additional p function was variationally determined to be 0·25 a_0^{-2} at the intermediate OH_2–H^+ structure (O–H^+ = 1·3 Å and $\angle HOH^+ = 108{\cdot}6°$) which was the optimum structure at this O–H^+ separation. Then, we optimized the HOH angle of the OH_2 fragment at a few points on the reaction path. The results show that the geometrical change of the OH_2 fragment gives little effect on the driving force acting of H^+. We therefore proceed with our study using the results of the fixed OH_2 geometry.

In the second step, we have calculated the floating wavefunctions [5, 7] along the reaction path, using the minimal STO-3G basis having the same exponents. We have not floated all the basis AO's but only the 1s AO belonging to H^+, since in order that the force F_A acting on the nucleus A satisfies the Hellmann–Feynman theorem, it is sufficient that only the centres of the AO's belonging to the atom A be determined variationally [5]. The floating distance of the 1s(H^+) AO in the reaction process is given in table 1. It is large for the intermediate stage and relatively small for the initial and last stages. The floating always occurs ahead of H^+ (on the side of the O atom) and reflects the electron-cloud preceding [4 c, e] in the reaction process. The floating distance Δr has some parallelism with the force acting on H^+, especially with the AD force, as expected (see § 3.2 and figure 2 (*a*)).

Table 1. Floating distance of the 1s(H^+) AO in the reaction process $OH_2+H^+\rightarrow OH_3^+$.†

R/Å	Floating distance/Å		
	Δx	Δy	Δr
4·0	0·0	0·0047	0·0047
2·8	0·0267	0·0225	0·0350
2·0	0·0708	0·0498	0·0865
1·6	0·0627	0·0584	0·0857
1·3	0·0422	0·0546	0·0690
1·02	0·0107	0·0393	0·0407

† The x and y axes are defined in figure 1. The floating always occurs ahead of H^+ (on the side of the O atom). Δx and Δy denote the x- and y-directional distances between the centre of the 1s(H^+) AO and the position of the H^+, and $\Delta r = \sqrt{[(\Delta x)^2+(\Delta y)^2]}$.

In table 2, we have checked the accuracy of the forces obtained from the fixed AO wavefunction through comparison with the forces from the floating wavefunction. In the fixed AO method, the total driving force was calculated smaller throughout the reaction process. At $R = 2{\cdot}8$ and 1·6 Å (R denotes the O–H^+ distance), the accuracies of the total driving forces are 83 and 55 per cent, respectively. The overall accuracy is estimated to be 74 per cent from the proton affinities ΔE (total force) and ΔE(SCF). As seen in table 2, the dominant origin of this error is ascribed to the smallness of the AD force. The other force components are similar in magnitude in both fixed and floating calculations. (Though its contribution is small, the EC($H^+\cdots H$) force changed from repulsive (floating AO method) to attractive (fixed AO method). This may be due to the

Table 2. Comparison of the driving forces acting on the H^+ calculated from the fixed AO and floating 1s(H^+) AO wavefunctions at $R=2{\cdot}8$ and $1{\cdot}6$ Å†.

Force/$E_H a_0^{-1}$	$R=2{\cdot}8$ Å		$R=1{\cdot}6$ Å	
	Fixed AO's (minimal + p)	Floating 1s(H^+) (minimal)	Fixed AO's (minimal + p)	Floating 1s(H^+) (minimal)
AD force	−0·0147	−0·0220	−0·0346	−0·0957
EC(H^+–O) force	−0·0021	−0·0014	−0·0765	−0·0912
EC($H^+\cdots$H) force	−0·0005	+0·0001	−0·0035	+0·0062
EGC force	−0·0027	−0·0007	+0·0312	+0·0281
Total force	−0·0200	−0·0240	−0·0834	−0·1526

† The force component parallel to the O–H^+ axis is given in atomic units. The positive and negative signs correspond to repulsive and attractive forces, respectively.

diffuse polarization functions (exponent $0{\cdot}25\ a_0^{-2}$) which may allow some density accumulation in the nonbonding $H^+\cdots$H region.) The order of importance was calculated to be AD > EC(H^+–O) > EGC + EC($H^+\cdots$H) by the floating wavefunctions. However, in the fixed AO approximation, the order of the AD and EC(H^+–O) forces was interchanged in the range $1{\cdot}9 > R > 1{\cdot}5$ Å. The results of the floating wavefunction should be more reliable. In the following analysis, we use the results of the floating AO calculation.

3. Analysis of the reaction

3.1. *Reaction path*

The calculated minimum-energy reaction path is shown in figure 1. For $R > 4$ Å, the calculated path coincided with the C_{2v} axis of the OH_2 fragment. Namely, at large separations, the proton attacks the in-plane lone-pair MO (pσ orbital) of the OH_2. As R decreases, the proton shifts towards one of the lone-pair hybrids (hybrids between the pσ and pπ lone-pair MO's) and reaches the equilibrium geometry of oxonium ion OH_3^+. In the calculation for the $NH_2 + H \rightarrow NH_3$ reaction [3], the hydrogen atom attacks the singly-occupied pπ orbital of the NH_2 fragment, as expected from the SOMO–SOMO interaction [13]. In the present case, the HOMO–LUMO interaction suggests the pπ orbital be attacked [13], but actually the next HOMO, pσ orbital, seems to be attacked in the initial stage. This is a result of the sensitive balance in the electronic and nuclear factors; orbital interaction favours the pπ-attack, while the nuclear repulsion favours the pσ-attack. The potential energy curve along the reaction path was smooth and reasonable even in the dissociation limit (see figure 2 (*b*)). As was expected for the NH_2–H system, the calculated reaction path suggests the possibility of rotational excitation of the OH_2 fragment in the dissociation process $OH_3^+ \rightarrow OH_2 + H^+$.

During the reaction process, the forces which work to change the HOH angle and the O–H bond lengths have been induced on the H nucleus of the OH_2 fragment; these forces are given in table 3. The transverse force $F_{H\perp}$ works to increase the HOH angle; it increases as R decreases. This is in agreement with the experimental difference in the valence angles of OH_2 (105°) and OH_3^+

Table 3. Transverse and parallel forces acting on the H nucleus of the OH_2 fragment in the OH_2 plane†.

R/Å	Force on H/$E_H a_0^{-1}$	
	transverse‡	parallel§
∞	0·0288	0·0715
2·8	0·0285	0·0860
2·0	0·0332	0·0969
1·6	0·0339	0·1019
1·3	0·0341	0·1027
1·02‖	0·0125	0·0262

† The O–H bond length and HOH angle were fixed to those of water (0·96 Å, 105°) except for equilibrium OH_3^+ molecule.

‡ The positive force works to increase the HOH angle.

§ The positive force works to stretch the O–H bond.

‖ The equilibrium OH_3^+ molecule. O–H = 1·2 Å and HOH = 117°.

(117°), since here the angle was fixed to that of water except for the equilibrium OH_3^+ molecule. The force $F_{H\parallel}$ parallel to the O–H bond works to stretch the length ; it increases with the decrease in R. This result also explains the experimental difference in the bond lengths of OH_2 (0·96 Å) and OH_3^+ (1·02 Å), since the bond length was fixed to that of water. However, we note that these results are only semi-quantitative since the AO's on H's of the OH_2 fragment were not floated.

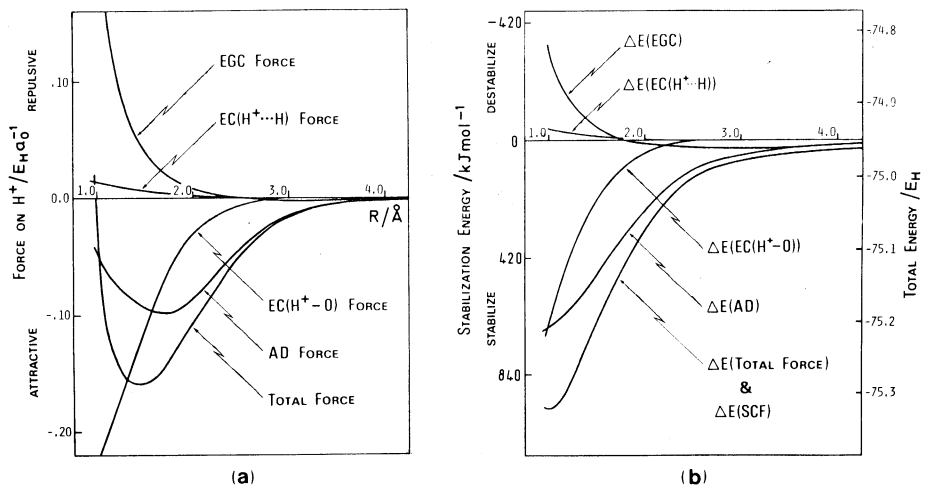

Figure 2. (*a*) The force acting on the approaching H^+. The force component parallel to the O–H^+ axis is plotted against R. (*b*) Partitioning of the stabilization energy based on the integrated H–F force. The stabilization energy due to the geometrical change of the OH_2 fragment at the equilibrium OH_3^+ molecule is not included. The curves for ΔE (total force) and ΔE(SCF) coincide each other.

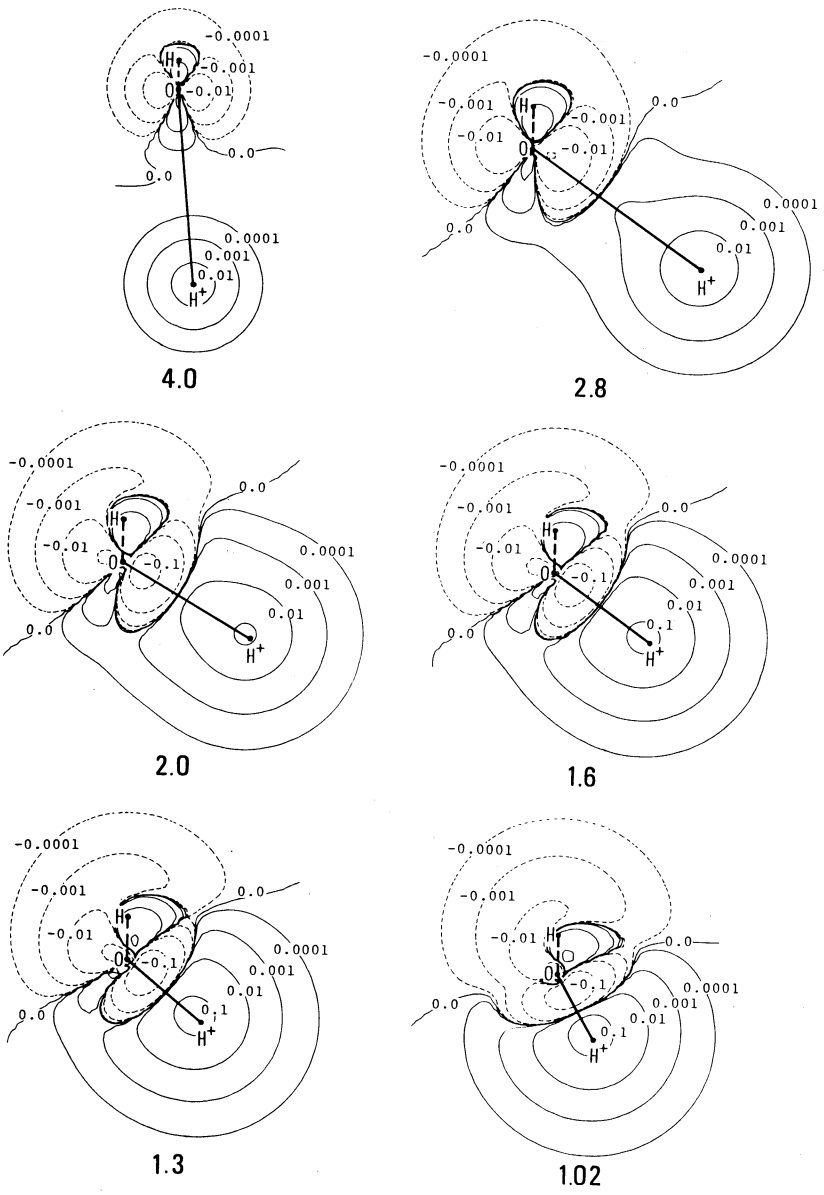

Figure 3. The density difference contour maps (in a_0^{-3}) for the OH_2–H^+ system at several O–H^+ distances. Solid lines and positive values mean the increase in the electron density relative to the separated system, while dashed lines and negative values the decrease in the electron density. The O–H^+ distances indicated below the maps are given in Å. The map for 4·0 Å is drawn in 2/3 scale relative to the other maps.

3.2. *Force and density origin of the reaction*

The force acting on the approaching proton is shown in figure 2 (*a*) as a function of R. We have plotted the force component parallel to the O–H^+ axis. Figure 2 (*b*) shows the energy curves obtained by integrating the Hellmann–Feynman force and its components. The ΔE (total force) curve coincides with the SCF-energy curve (ΔE(SCF)) since the present floating wavefunction satisfies the Hellmann–Feynman theorem. These energy curves permit direct investigation on the effects of the density reorganization on the stabilization energy of the system through Hellmann–Feynman force. In figure 2 (*a*), the total driving force gradually becomes attractive from $R\sim 4{\cdot}2$ Å, reaches its maximum at $\sim 1{\cdot}4$ Å, and vanishes at 0·99 Å (the minimum in the energy curve). We see in figures 2 (*a*) and 2 (*b*) that the reaction proceeds monotonously without reaction barriers. The equilibrium bond length (R_e) and the stretching force constant (k_e) were calculated to be 0·99 Å and 892 Nm^{-1}, respectively, while the corresponding experimental values are 1·02 Å (from the IR spectra of hydronium perchlorate and sulfate) [11] and 631 Nm^{-1} (from the Raman spectra of hydronium perchlorate crystal)[14], respectively. Accurate theoretical values for R_e and k_e are 0·959 Å and 849 Nm^{-1} (SCF), and 0·972 Å and 758 Nm^{-1} (CI) [18]. The proton affinity was obtained as 966 kJ mol^{-1} from the integration of the Hellmann–Feynman force ; it is larger than the experimental value 710–840 kJ mol^{-1} [14]. (Recent experimental studies have given the values 710 (high pressure mass spectrometry) [19 a] and 714 kJ mol^{-1} (pulsed ion cyclotron resonance) [19 b].)

Next, we study the origin of the reaction on the basis of the partitioned Hellmann–Feynman forces (figure 2 (*a*)), their density origins (figure 3), and their contributions to the stabilization energy (figure 2 (*b*)). As in the previous study for $NH_2+H\rightarrow NH_3$ [3], the reaction process is divided into the initial ($R>2{\cdot}5$ Å), intermediate ($2{\cdot}5>R>1{\cdot}5$ Å), and final ($1{\cdot}5$ Å $>R>R_e$) stages. We are interested in the differences in the origins between the ionic and radical reactions.

In the initial stage, the AD force is the dominant origin of the driving force, as seen in figures 2 (*a*), 2 (*b*), and 3. This AD force arises from the inward polarization of the electron cloud which is transferred from the lone pair of OH_2 to the atomic region of H^+. The extended gross charge (EGC) force, which is the origin of the attraction before charge transfer occurs, gives a secondary contribution in this range. The attractive EGC force is due mainly to the coulombic force between the H^+ and the negative gross charge on O. This is confirmed by the fact that the EGC force and the approximate gross charge (GC) force [4 a] are calculated to be nearly equal at large R. Figure 2 (*b*) shows that the stabilization energy due to this EGC force, ΔE (EGC), is important as well as that due to the AD force, ΔE(AD), particularly at large separations ($R>3{\cdot}5$ Å).

In the intermediate stage, the AD force is again a predominant origin of the driving force (see figure 2). The AD force is largest at $R\sim 1{\cdot}7$ Å, where we note that the floating distance of the 1s (H^+) AO is also largest (table 1). The predominance of the AD force in the intermediate stage seems to be characteristic of ionic reactions as we shall discuss later. The attractive EC(H^+–O) force increases rapidly from $R\sim 3$ Å. At $R\sim 1{\cdot}6$ Å, the AD and EC(H^+–O) forces give the same contributions and at shorter distances the latter dominates. The density origin of the EC(H^+–O) force is the electron cloud transferred and accumulated in the O–H^+ interatomic overlap region from the region around the

OH_2 (especially from one of the lone-pair hybrids). The stabilization energy due to the EC(H^+–O) force, ΔE(EC(H^+–O)), also increases rapidly (16 per cent of ΔE (total force) at $R=2$ Å and 67 per cent at $R=R_e$), but it does not exceed ΔE(AD) even at $R=R_e$. At $R\sim 2{\cdot}5$ Å, the EGC force changes from attractive to repulsive. In this stage, however, the repulsion is small compared to the attraction due to the AD and EC(H^+–O) forces, so that the reaction is further accelerated.

In the last stage, the repulsive EGC force, which has increased rapidly from $R\sim 2{\cdot}5$ Å, terminates the reaction at $R=0{\cdot}99$ Å (figure 2 (*a*)). This is due to the repulsion of the incompletely shielded nuclei in the OH_3^+ system. The repulsive EGC force works to destabilize the system (figure 2 (*b*)). At the equilibrium structure, the stabilization energies due to the AD and EC(H^+–O) forces reach as much as 668 and 651 kJ mol^{-1}, respectively, while the destabilization energy due to the EGC force is -311 kJ mol^{-1}. The EC($H^+\cdots$H) force between the non-bonding H^+ and H atoms is small and repulsive throughout the reaction. This force is parallel to the so-called exchange repulsion and contributes to destabilize the system by -42 kJ mol^{-1} at $R=R_e$. These stabilization and destabilization energies add up to the proton affinity of water (996 kJ mol^{-1}), and mean that the origin of the proton affinity is both the inward electron-cloud polarization in the atomic region (AD force) and the electron-cloud accumulation in the bond region (EC(H^+–O) force). This is different from previous systems [3, 4 b, 6], where only the latter is the dominant origin of the heat of reaction.

The process of O–H^+ bond formation, accompanied by the accumulation of electron density in this bond region, is illustrated in figure 4 using localized MO (LMO) [15] maps. It is interesting to note that at large separations, the O–H^+ bond LMO is essentially one of the two lone pairs of the OH_2 fragment. The map for 2·8 Å has the character of both the lone pair and bond pair. At 1·6 Å, the LMO map shows a typical profile of the bond orbital. Thus, the present reaction may be regarded as the transformation of the lone pair to the bond pair. The other lone-pair and O–H bond orbitals are shown to suffer little change ; this is also seen in the density difference maps (figure 3).

It is also interesting to compare the density reorganization of the present reaction system with the characteristics of the ionic bond studied by Bader *et al.* for diatomic molecules at their equilibrium bond lengths [16, 17]. Bader *et al.* suggested that in ionic molecules the transferred electron density is almost localized around the acceptor nucleus. Indeed, such trends of the electron density is observed for the equilibrium OH_3^+ molecule (see the map for $R=$ 1·02 Å in figure 3). However, in the intermediate stage of the reaction, the delocalization of the transferred density in the overlap region is also remarkable as well as the localization near the proton (maps for $R=2{\cdot}8$–$1{\cdot}6$ Å in figure 3). The electron density near the oxygen shows a deformed quadrupolar polarization [17] throughout the process. It occurs along the symmetry axis rather than the forming bond axis, as discussed in the previous study [3].

We now compare the results for the present system, $OH_2+H^+\rightarrow OH_3^+$, with those of the previous system, $NH_2+H\rightarrow NH_3$ [3]. In the initial stage, the dominant contribution of the AD force is common to both reactions. However, the role of the EGC force is different from the previous case, where the EGC force was always repulsive [3]. The attractive nature of the present EGC force

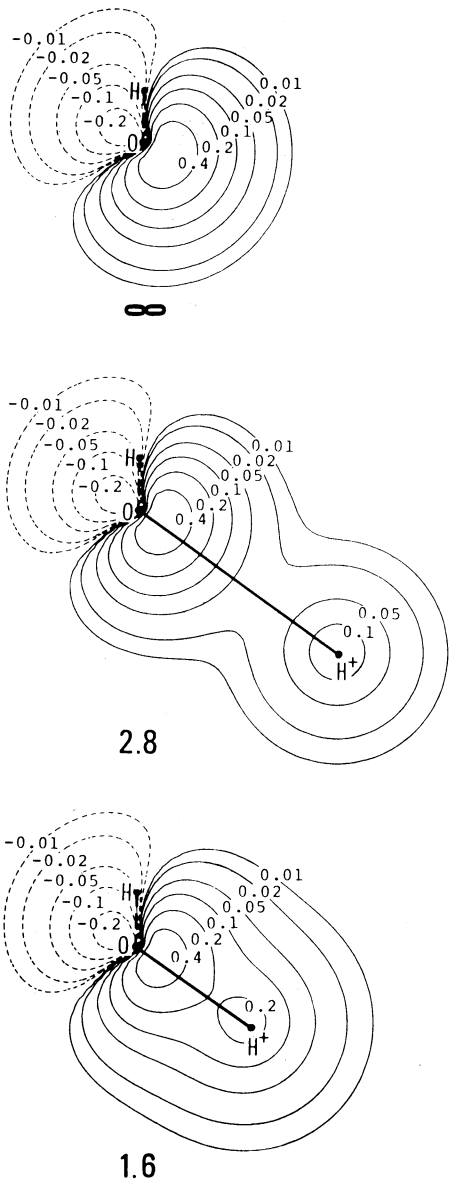

Figure 4. The O–H^+ bond LMO maps. The O–H^+ distances indicated below the maps are given in Å.

reflects the ionic nature of the reaction as mentioned before. In the intermediate and last stages, the dominant factor of the driving force is different for these two reactions. In table 4, we have compared the driving forces for the reactions $OH_2+H^+\rightarrow OH_3^+$ and $NH_2+H\rightarrow NH_3$, calculated at the same distance, $R=2{\cdot}0$ Å in the intermediate stage. Although the results from the fixed AO wavefunctions have been used, the parallelism between the floating and fixed AO results for the OH_3^+ system suggests that the characteristics of the reactions

Table 4. Comparison of the driving forces of the reactions $OH_2+H^+ \rightarrow OH_3^+$ and $NH_2+H \rightarrow NH_3$ at R=2·0 Å†‡.

Force/$E_H G_0^{-1}$	Force on H^+ (OH_2–H^+ system)		Force on H (NH_2–H system)
	floating 1s(H^+)	fixed AO's	fixed AO's
AD force	−0·084 (81)	−0·038 (61)	−0·012 (33)
EC(H^+–O) or EC(H–N) force	−0·031 (29)	−0·029 (46)	−0·021 (57)
EC(H^+···H) or EC(H···H) force	+0·002 (−2)	−0·005 (7)	−0·008 (22)
EGC force	+0·009 (−8)	+0·009 (−14)	+0·004 (−12)
Total force	−0·104 (100)	−0·063 (100)	−0·037 (100)

† For the fixed AO wavefunctions, the minimal STO-3G plus p basis was used. For the floating 1s(H^+) wavefunction, see text.

‡ Values in parentheses are per cent ratios.

are retained in the fixed AO calculations at this distance. We find, in table 4, that the AD force is a dominant origin of the driving force for the OH_2+H^+ reaction (AD dominance), while the EC force is for the NH_2+H reaction (EC dominance). This was also confirmed from the stabilization energies obtained by the direct force integrations. For ionic bonds, Bader *et al.* [16, 17] suggested that the localized atomic density should be polarized by the electric field of the other ionic atoms. The predominant contribution of the AD force in the OH_2+H^+ reaction seems to be in accord with their statement. In the NH_2–H system, however, the reaction is essentially covalent, so that a larger contribution of the EC(H–N) force may follow. The same is true for the reactions $H+H \rightarrow H_2$ and $2CH_3 \rightarrow C_2H_6$. Therefore, the AD and EC dominances seem to be of some parallelism with the ionic and covalent nature of the reactions, respectively. This also agrees with the results of Bader *et al.* for diatomic molecules [16, 17]. In density language, the electron-cloud preceding [4 c, e] is commonly the origin of the driving force of the reactions, but it may occur predominantly in the atomic region for the ionic case while in the bond region for the covalent case. However, this point should be examined by extensive calculations.

Lastly, we note the following. Despite the fact that the reactant H^+ has no electrons which contribute to bond formation, the EC(H^+–O) force curve resembles the previous EC(H–N) force curve in their behaviour ; their attraction begins at about 2·8 Å and then rapidly increases. These results for the AD and EC(H^+–O) forces show that in the OH_2–H^+ system the electron transfer occurs quite effectively from the OH_2 fragment (especially from one of the lone pairs) into the H^+ atomic region and the O–H^+ bond region. Indeed, the population of H^+ amounts to 0·126 even at $R=4{\cdot}0$ Å ; then it reaches 0·596 at $R=R_e$.

We acknowledge Messrs K. Kondo and K. Matsuda for their computational assistance. We also express our appreciation to the Data Processing Center of Kyoto University for the use of FACOM 230–75 computer. Part of this study has been supported by the Scientific Research Grants from the Ministry of Education.

References

[1] Hellmann, H., 1937, *Einführung in die Quantenchemie* (Deuticke) ; Feynman, R. P., 1939, *Phys. Rev.*, **56,** 340.

[2] (a) Deb, B. M., 1973, *Rev. mod. Phys.*, **45,** 22. (b) Deb, B. M. (editor), *The Force Concept in Chemistry* (Van Nostrand Reinhold) (in the press).

[3] Nakatsuji, H., Koga, T., Kondo, K., and Yonezawa, T., 1978, *J. Am. chem. Soc.*, **100,** 1029.

[4] (a) Nakatsuji, H., 1973, *J. Am. chem. Soc.*, **95,** 345, 354, 2084. (b) Nakatsuji, H., Kuwata, T., and Yoshida, A., 1973, *Ibid.*, **95,** 6894. (c) Nakatsuji, H., 1974, *Ibid.*, **96,** 24, 30 ; (d) Nakatsuji, H., and Koga, T., 1974, *Ibid.*, **96,** 6000. (e) Nakatsuji, H., and Koga, T., chapter 4 of reference [2 b].

[5] Nakatsuji, H., Matsuda, K., and Yonezawa, T., 1978, *Chem. Phys. Lett.*, **54,** 347 ; 1978, *Bull. chem. Soc. Japan*, **51,** 1315. Nakatsuji, H., Kanayama, S., Harada, S., and Yonezawa, T., 1978, *J. Am. chem. Soc.*, **100,** 7528.

[6] (a) Bader, R. F. W., and Chandra, A. K., 1968, *Can. J. Chem.*, **46,** 953. (b) Chandra, A. K., and Sunder, R., 1971, *Molec. Phys.*, **22,** 369. (c) Chandra, A. K., and Sebastian, K. L., 1976, *Chem. Phys. Lett.*, **41,** 593 ; *Molec. Phys.*, **31,** 1489.

[7] Hurley, A. C., 1954, *Proc. R. Soc.* A, **226,** 170, 179, 193 ; 1964, *Molecular Orbitals in Chemistry, Physics, and Biology*, edited by P.-O. Löwdin and B. Pullmann (Academic Press).

[8] Hirschfelder, J. O., and Eliason, M. A., 1967, *J. chem. Phys.*, **47,** 1164.

[9] Deb, B. M., 1974, *J. Am. chem. Soc.*, **96,** 2030 ; 1975, *Ibid.*, **97,** 1988. Deb, B. M., Sen, P. N., and Bose, S. K., 1974, *J. Am. chem. Soc.*, **96,** 2044.

[10] Herzberg, G., 1966, *Molecular Spectra and Molecular Structure. III. Electronic Spectra and Electronic Structure of Polyatomic Molecules* (Van Nostrand).

[11] Zundel, G., 1969, *Hydration and Intermolecular Interactions* (Academic Press). Richards, R. E., and Smith, J. A. S., 1952, *Trans. Faraday Soc.*, **48,** 307, 675. Savoie, R., and Giguere, P. A., 1964, *J. chem. Phys.*, **41,** 2698.

[12] (a) Stewart, R. F., 1970, *J. chem. Phys.*, **52,** 431. (b) Hehre, W. J., Stewart, R. F., and Pople, J. A., 1969, *J. chem. Phys.*, **51,** 2657.

[13] Fukui, K., 1970, *Theory of Orientation and Stereoselection* (Springer-Verlag).

[14] A brief review on the structure, force constants, and proton affinity of OH_3^+ molecule is given in : Bishop, D. M., 1965, *J. chem. Phys.*, **43,** 4453.

[15] Edmiston, C., and Ruedenberg, K., 1963, *Rev. mod. Phys.*, **35,** 457.

[16] Bader, R. F. W., and Henneker, W. H., 1965, *J. Am. chem. Soc.*, **87,** 3063. Bader, R. F. W., Henneker, W. H., and Cade, P. E., 1967, *J. chem. Phys.*, **46,** 3341. Bader, R. F. W., Keaveny, I., and Cade, P. E., 1967, *Ibid.*, **47,** 3381. Bader, R. F. W., and Bandrauk, A. D., 1968, 1968, *Ibid.*, **49,** 1653.

[17] Bader, R. F. W., qnd Bandrauk, A. D., 1968, *J. chem. Phys.*, **49,** 1666. Bader, R. F. W., Keaveny, I., and Runtz, G., 1969, *Can. J. Chem.*, **47,** 2308. Bader, R. F. W., and Ginsberg, J. L., 1969, *Can. J. Chem.*, **47,** 3061.

[18] Diercksen, G. H. F., and Kraemer, W. P., 1975, *Theor. chim. Acta*, **36,** 249.

[19] (a) Yamdagni, R., and Kebarle, P., 1976, *J. Am. chem. Soc.*, **98,** 1320. (b) Wolf, J. F., Staley, R. H., Koppel, I., Taagepera, M., McIver, R. T., Jr., Beauchamp, J. L., and Taft, R. W., 1977, *J. Am. chem. Soc.*, **99,** 5417.